Bornavirus encephalitis shows a characteristic magnetic resonance phenotype in humans

Tom Finck, Friederike Liesche Starnecker, Monika Probst, Stefanie Bette, Viktoria Ruf, Christina Wendl, Franziska Dorn, Klemens Angstwurm, Jürgen Schlegel, Claus Zimmer, Benedikt Wiestler, Isabel Wiesinger

Angaben zur Veröffentlichung / Publication details:

Finck, Tom, Friederike Liesche Starnecker, Monika Probst, Stefanie Bette, Viktoria Ruf, Christina Wendl, Franziska Dorn, et al. 2020. "Bornavirus encephalitis shows a characteristic magnetic resonance phenotype in humans." *Annals of Neurology* 88 (4): 723–35. https://doi.org/10.1002/ana.25873.

Bornavirus Encephalitis Shows a Characteristic Magnetic Resonance Phenotype in Humans

Tom Finck, MD,[1†] Friederike Liesche-Starnecker, MD,[2†] Monika Probst, MD,[1] Stefanie Bette, MD,[3] Viktoria Ruf, MD,[4] Christina Wendl, MD,[5] Franziska Dorn, MD,[6] Klemens Angstwurm, MD,[7] Jürgen Schlegel, MD,[2] Claus Zimmer, MD,[1] Benedikt Wiestler, MD,[1‡] Isabel Wiesinger, MD,[5‡] and the Bornavirus-Encephalitis Study Group

Objective: The number of diagnosed fatal encephalitis cases in humans caused by the classical Borna disease virus (BoDV-1) has been increasing, ever since it was proved that BoDV-1 can cause human infections. However, awareness of this entity is low, and a specific imaging pattern has not yet been identified. We therefore provide the first comprehensive description of the morphology of human BoDV-1 encephalitis, with histopathological verification of imaging abnormalities.

Methods: In an institutional review board-approved multicenter study, we carried out a retrospective analysis of 55 magnetic resonance imaging (MRI) examinations of 19 patients with confirmed BoDV-1 encephalitis. Fifty brain regions were analyzed systematically (T1w, T2w, T2*w, T1w + Gd, and DWI), in order to discern a specific pattern of inflammation. Histopathological analysis of 25 locations in one patient served as correlation for MRI abnormalities.

Results: Baseline imaging, acquired at a mean of 11 ± 10 days after symptom onset, in addition to follow-up scans of 16 patients, revealed characteristic T2 hyperintensities with a predilection for the head of the caudate nucleus, insula, and cortical spread to the limbic system, whereas the occipital lobes and cerebellar hemispheres were unaffected. This gradient was confirmed by histology. Nine patients (47.4%) developed T1 hyperintensities of the basal ganglia, corresponding to accumulated lipid phagocytes on histology and typical for late-stage necrosis.

Interpretation: BoDV-1 encephalitis shows a distinct pattern of inflammation in both the early and late stages of the disease. Its appearance can mimic sporadic Creutzfeldt–Jakob disease on MRI and should be considered a differential diagnosis in the case of atypical clinical presentation.

ANN NEUROL 2020;88:723–735

View this article online at wileyonlinelibrary.com. DOI: 10.1002/ana.25873

Received May 20, 2020, and in revised form Aug 5, 2020. Accepted for publication Aug 7, 2020.

Address correspondence to Dr Wiesinger, MD, Department of Radiology, Center of Neuroradiology, University Hospital Regensburg, Regensburg, Germany. E-mail: isabel.wiesinger@medbo.de

[†]T.F. and F.L.-S. contributed equally

[‡]I.W. and B.W. contributed equally

From the [1]Department of Diagnostic and Interventional Neuroradiology, Klinikum rechts der Isar, Technische Universität München, Munich, Germany; [2]Department of Neuropathology, Klinikum rechts der Isar, Technische Universität München, Munich, Germany; [3]Department of Diagnostic and Interventional Radiology and Neuroradiology, Augsburg University Hospital, Augsburg, Germany; [4]Center for Neuropathology and Prion Research, Ludwig-Maximilians-Universität München, Munich, Germany; [5]Department of Radiology, Center of Neuroradiology, University Hospital Regensburg, Regensburg, Germany; [6]Department of Diagnostic and Interventional Neuroradiology, Ludwig- Maximilians-Universität München, Munich, Germany; and [7]Department of Neurology, Regensburg University Hospital, Regensburg, Germany

Additional supporting information can be found in the online version of this article.

Introduction

Recently, it has been demonstrated that the classical Borna disease virus (BoDV-1; species *Mammalian 1 orthobornavirus*) can lead to encephalitis in humans that is usually fatal.[1–4] Consequently, the numbers of both retrospectively detected and recent cases are increasing.[5] To date, a lack of awareness of the disease and its clinical spectrum delay correct diagnosis and impede adequate therapy.

In animals, including horses and sheep, in which BoDV-1 infection has been known for centuries, typical neurological manifestations and distribution patterns have broadly been described.[6,7] For the most part, behavioral changes, including leg crossing and scratching, are observed. In the late stage, paralysis, blindness, and coma resulting in death occur in most cases.[6] Typically, the olfactory bulbs and hippocampus are affected, explaining why the olfactory system is believed to be a possible entry point in animals.[7]

In humans, the disease often starts with unspecific flu-like symptoms, followed by a broad variety of neurological symptoms, including gait ataxia, dysphagia, blurred speech, epileptic seizures, and hemiparesis.[5] A systematic neuropathological analysis of autopsy material of 6 patients with confirmed BoDV-1 encephalitis provided the first hints that the distribution pattern might differ from what we know in animals. An accentuation of the basal nuclei was described for two deceased patients.[1] Analysis of autopsy material is, however, limited by the fact that only the end stage of the disease can be evaluated. Life-prolonging therapies might have influenced these findings, especially regarding the distribution pattern. In contrast, magnetic resonance imaging (MRI) offers the chance to follow the course of the disease to gain a better understanding of the starting point and spread of the inflammation. From this point of view, discerning a specific pattern on MRI could accelerate the identification of affected patients and thus facilitate differentiation from other rapidly deteriorating conditions, such as similar encephalitis pathogens or prion-related disease.

Patients and Methods

Data Acquisition and Virus Detection

Ii this study, we evaluated 55 brain MRI examinations from 19 patients with confirmed postmortem diagnosis of human BoDV-1 encephalitis and included data from 4 university hospitals, one general hospital, and two community hospitals in southern Germany. No spinal imaging was available for review. For all patients, the presence of BoDV-1 RNA had been confirmed by reverse transcriptase quantitative polymerase chain reaction (RT-qPCR), as described earlier.[3] Additionally, in 13 patients, the diagnosis of BoDV-1 encephalitis was corroborated by immunohistochemistry against the nucleoprotein of BoDV-1 and BoDV-1 RNA in situ hybridization of brain tissue samples, as described previously.[1] Removal of patient-linked metadata and defacing of the MRI images for anonymization took place before evaluation of scans. Although data on Patient 4 (P3 of Liesche and colleagues[1]), Patient 7 (P2 of Liesche and colleagues[1]; P6 of Coras and colleagues[2]), Patient 8 (P1 of Liesche and colleagues[1]; Recipient 2 of Schlottau and colleagues[3]), Patient 9 (P5 of Liesche and colleagues[1]]), Patient 16 (P4 of Liesche and colleagues[1]; P7 Coras and colleagues[2]), Patient 11 (Recipient 1 of Schlottau and colleagues[3]), Patient 14 (P2 Coras and colleagues[2]), Patient 15 (P6 of Liesche and colleagues[1]; P8 Coras and colleagues[2]), and Patient 17 (P3 Coras and colleagues[2]) have been reported previously, the focus in the preceding studies was set on clinical information and not imaging findings. The local ethic committees of the respective institutions approved this retrospective study (577/19 S-SR and 560/19 S-KH).

Systematic Scan Evaluation

The magnetic resonance (MR) images were analyzed retrospectively, independently and in random order, by two neuroradiologists (T.F and I.W., with MRI experience of 3 and 7 years, respectively) blinded for the scanning time point or any clinical data beyond the fact that diagnosis of BoDV-1 encephalitis had been confirmed. A standardized scheme was defined to investigate 50 previously defined brain regions (a list of evaluated regions is given in supplementary Table S1) deemed anatomically and functionally relevant. After binary determination of whether a brain region showed any abnormalities, the intraparenchymal location of an anomaly into cortical, subcortical, deep white matter, or the basal ganglia was defined. Next, the morphology and quality of a particular lesion were classified based on its delineation, mass effect, and signal alterations on T1w/T2w/T2*w, lack/presence of diffusion restriction, lack/presence of contrast enhancement, or any combination of these signal changes. Raters were also asked to determine whether changes were suggestive of laminar necrosis, as defined by native T1 hyperintensity of the cortical band.[8] In divergent primary ratings, a consensus rating was reached by involving a third neuroradiologist (M.P.) with 10 years of experience.

Histopathology, Immunohistochemistry, and RNA In Situ Hybridization

From a representative patient for whom the formalin-fixed whole-brain specimen was available (bilateral if applicable and not specified otherwise), tissue samples from 25 locations (head of the caudate nucleus, striatum, globus pallidus, insula, thalamus [right], hippocampus [left],

occipital cortex, frontal cortex [right], parietal cortex [left], cerebellar vermis, cerebellar hemisphere, deep white matter [occipital], temporal pole [right], mesencephalon, and leptomeninx) were retrieved for histopathological evaluation. After paraffin embedding, 2µm-thick sections were sliced and stained with Hematoxylin and Eosin (H&E).

For immunohistochemistry, an established avidin–biotin complex technique was performed. Pretreatment in pH 6.0 citrate buffer at 95°C for 30 minutes for epitope uncovering and H_2O_2 were followed by overnight incubation with the primary antibodies against GFAP (Dako Denmark A/S, Glostrup, Denmark; polyclonal, rabbit, dilution 1:500), Iba1 (abcam, Berlin, Germany; polyclonal, rabbit, dilution 1:500), CD45 (DCS Innovative Diagnostik-Systeme, Habmurg, Germany; monoclonal, mouse, clones 2B11 and PD7/26, dilution 1:250) and CD68 (Dako Denmark A/S, Glostrup, Denmark; monoclonal, mouse, clone KP1, dilution 1:1,500).

For evaluation of virus distribution, a monoclonal antibody against the nucleoprotein of BoDV-1 was used, as described previously.[1] Afterwards, biotinylated secondary antibodies were applied for 30 minutes, followed by incubation with avidin-biotin-complex and diaminobenzidine reagents. Finally, counterstaining with Hematoxylin was conducted. Additionally, BoDV-1 RNA in situ hybridization with the probe V-BoDV1-G targeting 2-969 of NC_001607-1:2236-3747 (RNAscope; Advanced Cell Diagnostics, Newark, CA) was performed on a selection of 11 locations (bilateral if applicable and not specified otherwise; head of the caudate nucleus, striatum [right], insula, thalamus, hippocampus, parietal cortex [right], occipital cortex [left], frontal cortex [left], cerebellar vermis, cerebellar tonsils, and mesencephalon) as described previously.[9] Positive controls served as quality assurance for all immunohistochemical stains and the RNA in situ hybridization.

Histopathological Evaluation

Histopathological evaluation was performed by a highly experienced neuropathologist (F.L.-S.). The density of pathognomic Joest–Degen bodies[10] was determined by counting the number of inclusions in 10 high-power fields (HPFs; ocular: ×10/23; objective: ×40/0.75). The severity of edema was evaluated semiquantitatively by establishing a score ranging from 0 (no edema) via 1 (mild) and 2 (moderate) to 3 (severe edema). The virus distribution was evaluated by counting BoDV-1$^+$ cells in immunohistochemistry, extrapolating to a standardized tissue size of 1cm^2. Furthermore, cells with positive BoDV-1 RNA signal were counted and also standardized to a tissue size of 1cm^2.

For the evaluation of reactive astrogliosis and activated microglial cells, the average of GFAP$^+$ (GFAP is defined as glial fibrillary acidic protein) reactive astrocytes and Iba1$^+$ (IBA1 is defined as ionized calcium-binding adapter molecule 1) activated microglial cells, respectively, was calculated in 5 HPFs. All diffusely distributed CD45$^+$ lymphocytes and CD68$^+$ macrophages were counted and extrapolated. Furthermore, the severity of perivascular infiltration was determined by counting perivascularly located CD45$^+$ cells in 5 transversely cut vessels with similar diameter.

Twenty-five brain regions of Patient 4, who was included in a previous study,[1] were analyzed regarding the severity of edema, astrogliosis, microglial activation, and inflammation, in addition to detection of BoDV1 nucleoprotein and RNA. Given that some regions were covered by several samples, for statistics, the results were pooled to 14 relevant areas. From the aforementioned histopathological parameters, the general histopathology score was designed to provide a rough comparison of the inflammatory activity within different brain regions. For this purpose, all 14 areas received points for their rank regarding the 5 categories, with the highest score of 14 for the top rank and a score of 1 for the lowest rank. The ranking scores of the 5 parameters were summed to yield a general histopathology score.

Results

Patient and Scan Data

Complete clinical information was available for 18 of the 19 included patients (mean age 45 ± 23 [range 11–78] years; detailed clinical data are given in Table 1). Death occurred in all patients with available data at a mean of 38 ± 22 days after symptom onset. Three patients were under immunosuppressive therapy (P8, P11, and P14), whereas the other 16 patients had no relevant underlying medical conditions. Fever or flu-like episodes were the most common initial symptoms, apparent in 15 patients. Ascending tetraparesis (P8), progressive encephalopathic symptoms (P11), and dysarthria and visual hallucinations (P17) were the main symptoms on admission of the 3 other patients for whom clinical information was available. All patients lived in southern Germany, a region endemic for BoDV-1.

A total of 55 MRI scans from the 19 patients (mean scans per patient = 3.0 [range 1–4]) were available for analysis. All scans included a T2-weighted or fluid-attenuated inversion recovery (FLAIR) sequence of diagnostic quality; 46 (84%) examinations had diffusion imaging, and 46 (84%) examinations were contrast enhanced. Fourteen patients were scanned exclusively on 1.5T machines, 4 patients on 3T machines, and 1 patient (P2) was scanned on a 1.5T machine for baseline and a 3T machine for follow-up imaging.

TABLE 1. Summary of Clinical Data

Patient	Age at Death, yr	Symptoms at Admission	CSF Findings (Days after Symptom Onset)	Time Until Death, days
1	40–44	Fever, apathy, soporous state	Pleocytosis (4)	26
2	10–14	Fever, reduced general state, emesis, gait ataxia, enuresis	Pleocytosis (5)	28
3	70–74	Flu-like, with weakness of the limbs	Pleocytosis (6)	12
4	10–14	Flu-like, with fever; subsequently, altered general state, headaches, nystagm, gait ataxia, slurred speech and vestibular disorder	Pleocytosis, high protein, glucose and lactate (3)	25
5	10–14	Fever, seizures, somnolence	Pleocytosis, high protein and lactate, oligoclonal bands, mildly impaired blood–CSF barrier (24)	31
6	50–54	Fever, progressive confusion syndrome	Pleocytosis, oligoclonal bands, high protein (19)	45
7	20–24	Flu-like, with fever, headaches, arthralgia, apathy, memory dysfunction	Pleocytosis, oligoclonal bands, intrathecal IgM synthesis, elevated 14-3-3 protein (11)	39
8	70–74	Ascending tetraparesis, intention tremor of the arms	Pleocytosis, impaired blood–CSF barrier, elevated 14-3-3 protein (37)	96
9	75–79	Fever, productive cough, reduced general state, with unsteady gait and hemiparesis of the right side	Pleocytosis, high protein and lactate (2)	25
10	45–49	Flu-like, with headaches, disorientation	Pleocytosis, impaired blood–CSF barrier, elevated 14-3-3 protein (15)	39
11	65–69	Axonal polyneuropathy, progressive encephalopathic syndrome (or symptoms)	Impaired blood–CSF barrier, no pleocytosis (5)	42
12	30–34	Flu-like, with headaches	Pleocytosis, high lactate, impaired blood–CSF barrier (4)	31
13	35–39	Fever, dizziness, nausea, vertigo	Pleocytosis, high lactate, impaired blood–CSF barrier (3)	53
14	40–44	Flu-like, with headaches and progressive dizziness	Pleocytosis, high lactate, impaired blood–CSF barrier (4)	67
15	55–59	Flu-like, with progressive delirium	Pleocytosis, high lactate, impaired blood–CSF barrier (12)	16
16	15–19	Flu-like, with headaches, dizziness, ataxia, and seizures	Pleocytosis, high lactate and protein, elevated 14-3-3 protein (9)	12
17	65–69	Reduced general state, dysarthria, visual hallucinations	Pleocytosis, impaired blood–CSF barrier, intrathecal IgG synthesis (7)	74
18	30–34	Flu-like, abdominal pain	Pleocytosis (5)	48
19	70–75	Flu-like, confusion	NA	NA

In conformity with pseudonymization policies, patient age is provided only in 5-year intervals.
CSF = cerebrospinal fluid; NA = no information available; Pleocytosis refers to lymphomonocytic pleocytosis.

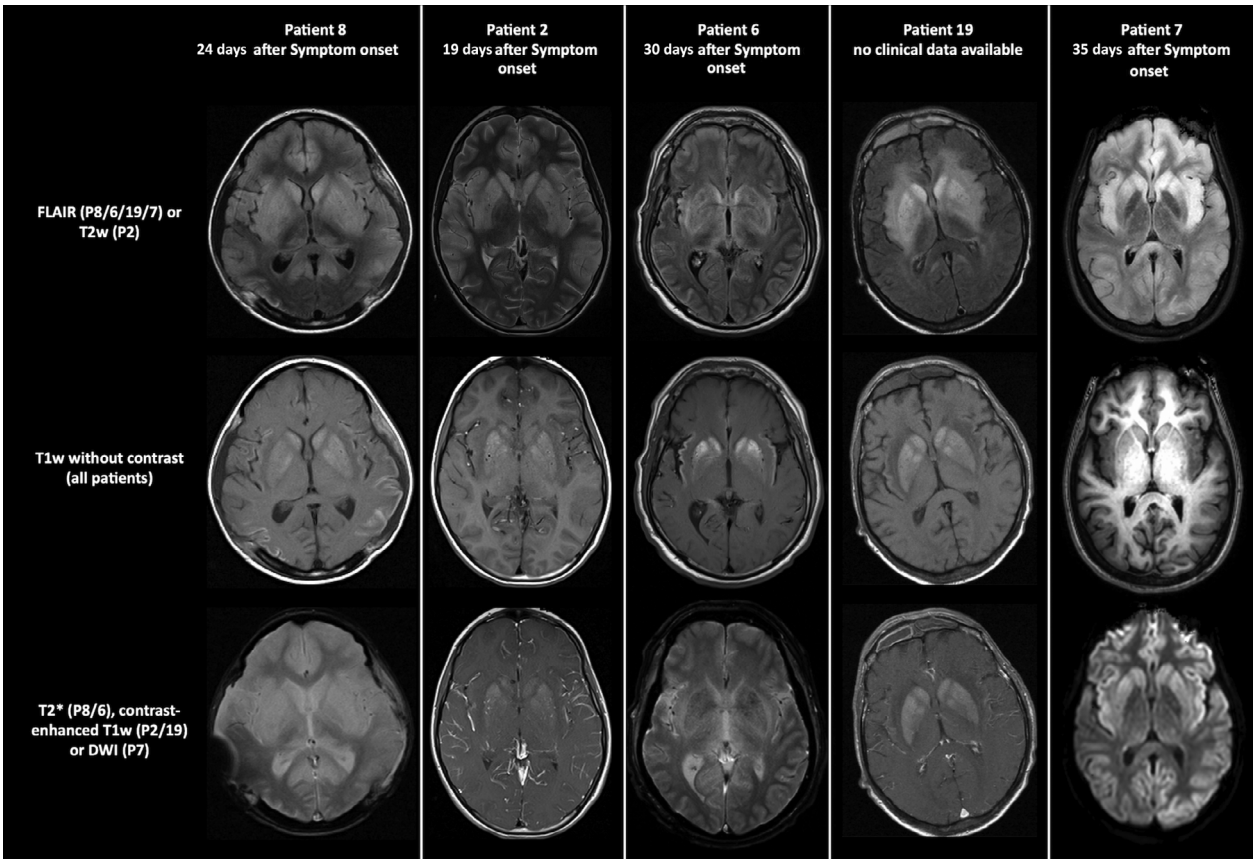

FIGURE 1: Representative magnetic resonance imaging data of 5 patients (for clinical information, refer to Table 1) with the typical imaging pattern for Borna disease virus (BoDV-1) encephalitis. Note the symmetrical distribution of T2-hyperintense (all patients) and occasional diffusion-restricted (Patient 7) changes in the basal ganglia, with spread to the insular ribbon and adjacent cortical band but sparing the occipital lobe (Patient 8) and cerebellar hemispheres (not shown). T1-hyperintense transformation of the basal ganglia (middle row) is a characteristic finding in late-stage disease (all shown patients).

Pattern and Quantitative Changes on MRI

Of the 19 included patients, 10 (53%) showed imaging abnormalities on baseline MRI. In these scans, acquired at a mean of 11 ± 10 days after symptom onset, a characteristic phenotype was distinguishable, with inflammatory lesions mainly arising from the head of the caudate nucleus in addition to the adjacent insula, thalamus, and operculum in descending frequency. This distinguishable pattern remained intact on follow-up imaging, available for 16 patients at a mean of 26 ± 13 days after symptom onset, with a lesion peak in the head of the caudate nucleus and heterogeneous spread into the adjacent parenchyma and brainstem now becoming more pronounced. Notably, the regions furthest from the basal ganglia (ie, the occipital poles and cerebellar hemispheres) were spared, even in late-stage disease. Figure 1 shows representative examples of this pattern.

Altogether, abnormalities were present in 41 of the 55 included scans and were distributed symmetrically among both hemispheres in 32 (78%) scans. The lesions showed a laterality in 7 (17%) scans and were strictly unilateral in 2 (5%) scans.

Quantitative evaluation of all baseline scans revealed that the count of affected brain regions per patient ranged from 0 to 26, with a group mean of 6.1 ± 8.5 (12.2% of the 50 investigated anatomical areas). Cortical structures were affected in 7 (37%) patients, the subcortical white matter in 4 (21%) patients, the deep white matter in 4 (21%) patients, and the subcortical nuclei in 6 (32%) patients. Anatomically, there was a strong predilection for the basal ganglia and the limbic system, with lesions being most common in the head of the caudate nucleus (7 [37%] patients), insula (6 [32%] patients), and hippocampus and (posteromedially accentuated) thalamus (5 [26%] patients each).

Quantitative evaluation of all follow-up scans revealed that the number of affected brain regions per patient increased sharply to a group mean of 19.3 ± 13.3 (38.6% of the 50 investigated anatomical areas) and ranged from 0 to 42 per patient. Cortical structures were affected in 12 (75%) patients, the subcortical white matter in 4 (25%) patients,

TABLE 2. The 10 Most Frequently and 5 Least Frequently Affected Brain Regions on MRI, with their Respective Signal Alterations for Both Baseline Scans (n = 19) and Available Follow-up Scans (n = 16)

	Baseline (n = 19)					Last Scan (n = 16)				
Region	Any Lesion	T2 High	DWI High	T2 High + CE	T2 + DWI High	Any Lesion	T2 High	DWI High	T2 High + CE	T2 + DWI High
Most affected regions										
Head of the Caudate Nucleus	7 (36.8%)	5	0	1	1	13 (81.3%)	8	0	1	4
Hippocampus	5 (26.3%)	1	0	1	2	12 (75.0%)	8	0	1	3
Insula	6 (31.6%)	3	0	1	2	12 (75.0%)	6	0	1	5
Parahippocampal gyrus	5 (26.3%)	2	0	1	1	11 (68.8%)	8	0	1	2
Temporal pole	4 (21.1%)	2	0	1	1	11 (68.8%)	7	0	2	2
Thalamus	5 (26.3%)	2	0	1	2	11 (68.8%)	7	0	1	2
Frontal pole	1 (5.3%)	1	0	0	0	10 (62.5%)	7	0	1	2
Putamen	4 (21.1%)	3	0	1	0	10 (62.5%)	6	0	2	2
Gyrus rectus	2 (10.6%)	2	0	0	0	10 (62.5%)	8	0	0	2
Operculum	5 (26.3%)	3	0	1	1	9 (56.3%)	6	0	1	2
Least affected regions										
Deep white matter occipital	0 (0%)	0	0	0	0	1 (6.3%)	1	0	0	0
Occipital pole	0 (0%)	0	0	0	0	1 (6.3%)	0	0	0	1
Optic nerves	0 (0%)	0	0	0	0	1 (6.3%)	1	0	0	0
Pineal gland	0 (0%)	0	0	0	0	1 (6.3%)	1	0	0	0
Cerebellar hemisphere	1 (5.0%)	1	0	0	0	0 (0%)	0	0	0	0

the deep white matter in 7 (44%) patients, and the subcortical nuclei in 14 (88%) patients. By analogy to baseline scans, the head of the caudate nucleus (13 [81%] patients) was most commonly involved, followed by the hippocampus (12 [75%] patients) and insular ribbon (12 [75%] patients). For more detail, the 10 most-affected and 5 least-affected brain regions, with their associated signal changes for the baseline scan and follow-up scan, are presented in Table 2.

Laminar necroses were detectable in none of the index scans and in 5 (32%) patients on follow-up. A frequent phenomenon was the T1-hyperintense transformation of the basal ganglia, occurring in 9 (47%) patients at a mean of 11 $\pm$ 8 days before death.

Microhemorrhages, as defined by patchy T2* signal loss, were discernable in none of the 55 systematically evaluated scans.

Time Dependency on Imaging

The median "time-to-abnormality" on MRI was 12 (interquartile range: 5–21) days after symptom onset and 22 (interquartile range: 15–28) days before death. A pictogram outlining the time-dependent MRI changes is given in Figure 2 and confirms the above-mentioned inflammation pattern in early disease, with subsequent spread into the adjacent parenchyma.

Correlation with Neuropathology

To confirm that the patterns described reflect the pathology of human Borna encephalitis, we compared neuropathological changes in 25 brain regions from Patient 4, who was included in a previous study,[1] with imaging findings in an MR scan acquired 2 days before death (Fig 3). The MR scan showed a typical pattern, with T2 hyperintensity of

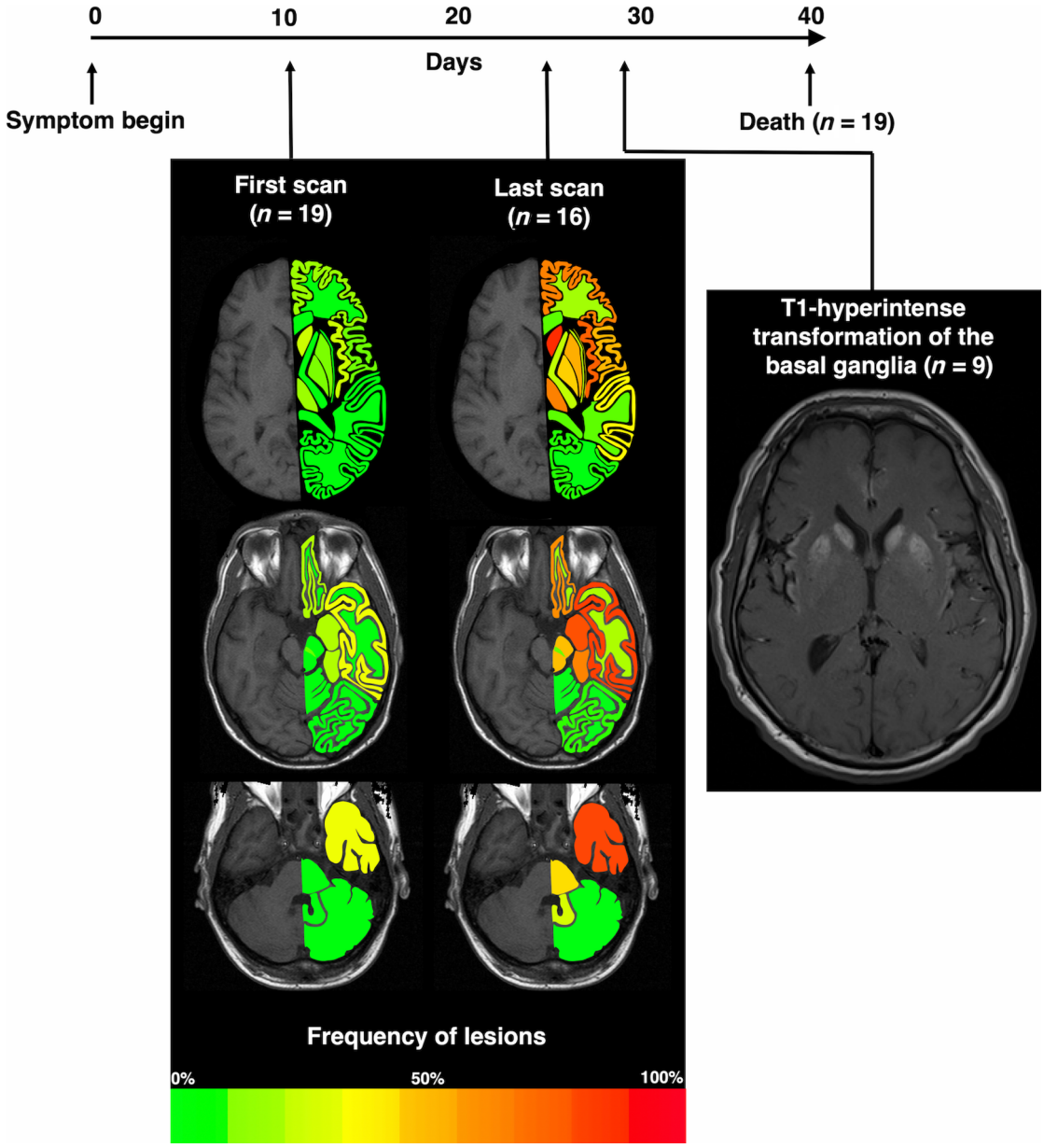

FIGURE 2: Pictograms with a color-based inflammation pattern of selected brain regions, illustrated for the first scan (available for 19 patients at a mean of 11 ± 10 days after symptom onset) and the follow-up scan (available for 16 patients at a mean of 26 ± 13 days after symptom onset). T1-hyperintense transformation of the basal ganglia was noted in 9 patients at a mean of 11 ± 8 days before death.

the basal ganglia, whereas the occipital lobe seemed not to be affected. In line with this observation, histology revealed marked changes in the basal ganglia, with strong perivascular and diffusely distributed $CD45^+$ lymphocytic infiltrates. GFAP- and Iba1-immunohistochemistry showed strong astroglial and microglial activation. Several cells with a positive signal for BoDV-1 RNA could be detected. In contrast, the occipital lobe showed only minimal inflammation. Nevertheless, it was notable that there were few perivascular lymphocytic infiltrates and the beginning of formation of microglial nodules.

To quantify the correlation between imaging and neuropathology, we defined a "general histopathology score," as explained in the Patients and Methods section. In this score, and by analogy to the aforementioned MRI phenotype, a clear pattern became evident, with the striatum and head of the caudate nucleus being most affected, followed by the limbic regions and insula. In contrast, and reproducing the gradient that was distinguishable on MRI, the cerebellar hemispheres and the occipital lobe showed the lowest inflammation. See Table 3 for the general histopathology score of each region.

Detailed quantitative readings showed that the highest number of Joest–Degen inclusion bodies was observed in the left striatum (7 of 10 HPFs), followed by the left head of the caudate nucleus and the frontal cortex (each 6 of 10 HPFs). The lowest numbers were seen in the cerebellar hemispheres (0 of 10 HPFs) and the samples of the occipital lobe (average 1 of 10 HPFs).

The highest edema score was reached in the temporal pole and parietal cortex (each scoring 3). No remarkable edema was detected in the cerebellar hemisphere (average score 0.5).

The highest number of reactive astrocytes was found in the thalamus (average 48.8 per HPF), followed by the striatum (average 41.8 per HPF) and the frontal cortex (average 40.8 per HPF). Notably, the activated astrocytes observed were often bizarrely enlarged and of gemistocytic and coarse appearance. The mildest astrogliosis was seen in the deep white matter (average 21.8 per HPF), mesencephalon (average 22 per HPF), and cerebellar hemispheres (average 23.7 per HPF).

The striatum showed the highest amount of activated microglial cells (average 199.2 per HPF), followed by the parietal cortex (average 102 per HPF). The cerebellar hemispheres (average 19.9 per HPF) and the occipital lobe (average 35 per HPF) were least affected by microglial activation.

Most diffusely distributed lymphocytes were present in the striatum (581 lymphocytes/cm^2) and the thalamus (486/cm^2). Frontal and parietal cortex showed least diffuse inflammation (41 and 44/cm^2, respectively). The strongest perivascular infiltrate was also seen in the striatum (average 75 per vessel) and the head of the caudate nucleus (average 68 per vessel). The lowest numbers were found in the cerebellar hemispheres (average 8 per vessel) and frontal cortex (average 19 per vessel).

Most BoDV-1 nucleoprotein$^+$ cells were detected in the striatum (128/cm^2) and the head of the caudate nucleus (103/cm^2), whereas the thalami and the cerebellar hemispheres were negative for the virus protein. The highest number of BoDV-1 RNA-positive cells was counted in the insula (158.3 positive cells/cm^2) and parietal

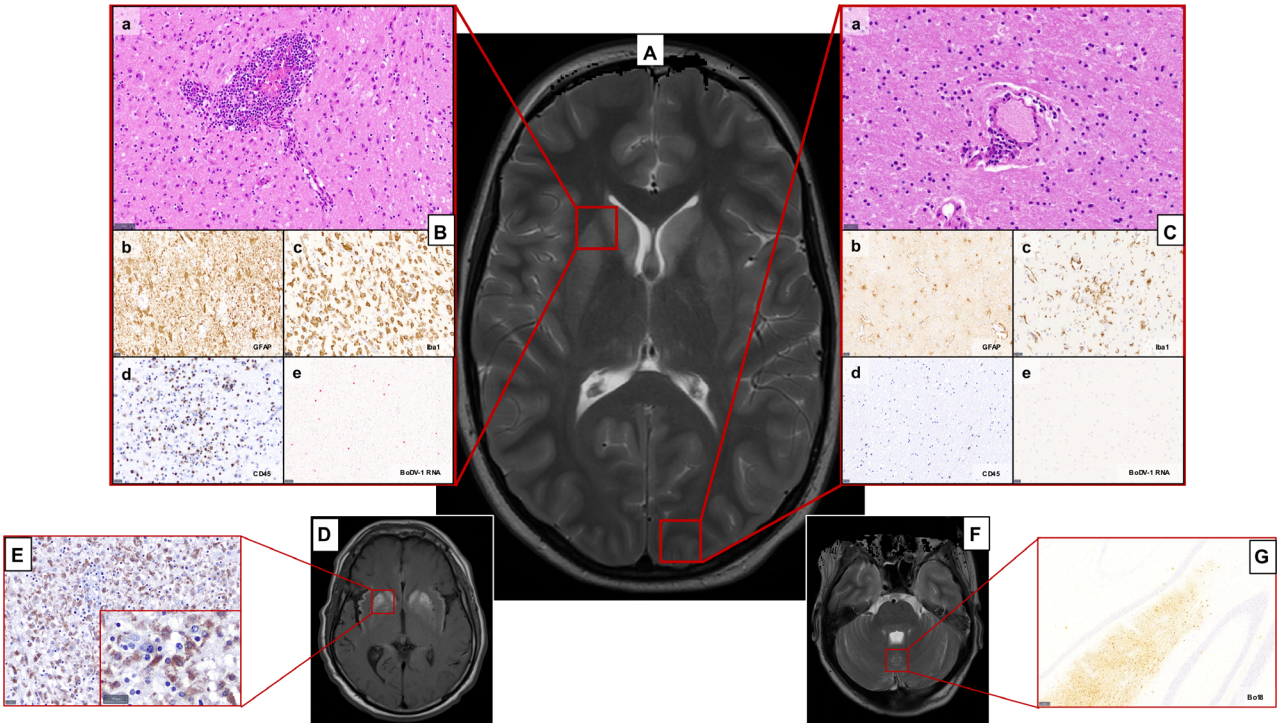

FIGURE 3: Comparison of histopathology with magnetic resonance imaging (MRI) abnormalities. (A) MRI of Patient 4 shows T2 hyperintensity of the basal ganglia, whereas the occipital lobe seems not to be affected. (B) In line with this observation, histology reveals marked changes in the basal ganglia, with strong perivascular (a) and diffusely distributed (d) CD45$^+$ lymphocytic infiltrates. GFAP- and Iba1-immunohistochemistry shows strong astroglial (b) and microglial activation. Several cells with a positive signal for Borna disease virus (BoDV-1) RNA can be detected (e). (C) In contrast, the occipital lobe shows only minimal inflammation. Nevertheless, it is notable that there are few perivascular lymphocytic infiltrates (a) and the start of formation of microglial nodules (c). (D, E) The histopathological correlate for the described strong T1-hyperintensity of the basal ganglia, shown in D, is a massive accumulation of CD68$^+$ macrophages, shown in E. (G) Note the fusiform positivity for BoDV-1 nucleoprotein (Bo18) in the cerebellar vermis, otherwise with complete negativity of the cerebellum (not shown), indicating an incipient infiltration by the virus. Scale bars: 50µm in Ba and Be; 200µm G; 20µm in all other panels.

TABLE 3. Degree of Pathology in Different Locations: Histopathological Analyses of Patient 4 Emphasize the Striatum and the Caput of the Caudate nucleus as Locations that are Mostly Affected in BoDV-1 Encephalitis, Whereas the Cerebellar Hemispheres and the Occipital Lobe are Least Affected

Localization	General Histopathology Score	BoDV-1$^+$ Cells, cells/cm^2 (rank)	Diffuse Lymphocytes, cells/cm^2 (rank)	Reactive Astrocytes, cells/HPF (rank)	Activated Microglial Cells, cells/HPF (rank)	Edema Score (rank)
Striatum	59	127.8 (13)	581.4 (14)	41.8 (13)	199.2 (14)	1.5 (5)
Caput of caudate nucleus	53	103.0 (12)	227.7 (11)	36.0 (10)	127.6 (13)	2.0 (7)
Hippocampus	47	68.5 (9)	293.9 (12)	35.2 (9)	95.2 (10)	2.0 (7)
Parietal lobe	45	82.7 (10)	44.1 (2)	34.8 (8)	102.0 (12)	3.0 (13)
Insula	40	27.1 (6)	104.3 (7)	36.5 (11)	95.0 (9)	2.0 (7)
Temporal lobe	40	9.2 (5)	55.1 (4)	32.6 (7)	97.4 (11)	3.0 (13)
Globus pallidus	39	60.9 (8)	168.5 (10)	30.5 (6)	88.5 (8)	2.0 (7)
Cerebellum, vermis	37	150.0 (14)	150 (9)	30.0 (5)	88.2 (7)	1.0 (2)
Thalamus	34	0.0 (1)	485.7 (13)	48.8 (14)	61.8 (4)	1.0 (2)
Frontal lobe	29	5.1 (4)	40.8 (1)	40.8 (12)	67.0 (5)	2.0 (7)
Deep white matter	25	84.6 (11)	117.3 (8)	21.8 (1)	53.4 (3)	1.0 (2)
Mesencephalon	25	33.9 (7)	52.1 (3)	22.0 (2)	74.2 (6)	2.0 (7)
Occipital lobe	10	0.9 (3)	89.5 (5)	23.8 (4)	35.0 (2)	1.5 (5)
Cerebellum, hemispheres	12	0.0 (1)	95.9 (6)	23.7 (3)	19.9 (1)	0.5 (1)

The general histopathology score was designed by adding the ranks of all 14 investigated locations (with the highest score of 14 for the top rank and a score of 1 for the lowest rank) regarding the 5-parameter detections of Borna disease virus (BoDV-1): nucleoprotein, diffuse lymphocytic infiltration, astrogliosis, activated microglia, and edema. The table shows the absolute numbers (average number cells per square centimeter or per high-power field [HPF], respectively), and the associated rank. For the evaluation of edema, the score (as described in the Patients and Methods section) is listed rather than an absolute number.

cortex (145.5/cm^2). No viral RNA was detected in the occipital and frontal cortex or in the cerebellar hemispheres.

Histopathological Correlate of T1 Hyperintensity of the Basal Ganglia

Given that a strong T1 hyperintensity of the basal ganglia developed in 9 patients, histopathological analysis was also focused on outstanding changes in this area. Remarkably massive accumulation of lipid phagocytes was observed in the basal ganglia of Patient 4. CD68$^+$ macrophages were also detected in other regions, but nowhere else at such high density, as illustrated further in Figure 3.

Discussion

Despite broad research surrounding BoDV-1 disease in horses and sheep, attention to the potential zoonotic spillover from the small mammal reservoir to humans has grown only recently, owing to the rising number of confirmed human infections in virus-endemic regions. As far as we know, BoDV-1 disease in humans shows strong similarities to the BoDV-1 infections in animals, with rapidly progressive symptoms and exceedingly high fatality rates.[1–4] A recently published retrospective analysis showed that a high fraction of initially non-classifiable fatal encephalitis cases was attributable to BoDV-1.[5] Given that clinical symptoms are often not

discernible from other neurological diseases, early identification of affected patients through widely available imaging would be most valuable to enable earlier engagement in potential therapies and to facilitate delineation from differential diagnoses. In this study, we provide the first comprehensive insight into the MRI abnormalities and their histopathologic correlates for the largest cohort so far of 19 patients with confirmed BoDV-1 encephalitis.

In agreement with the pre-reported viral tropism in animal models, we found a typical imaging pattern in both the early and late stages of human BoDV-1 disease.[11] As such, a distinct pattern of inflammation, with predominantly symmetric T2 hyperintensities affecting the head of the caudate nucleus, posteromedial thalamus, insular ribbon, and hippocampus in the early stages of disease, was clearly distinguishable on baseline MRI. In the later stages of the disease, this characteristic morphology remained intact as inflammation then spread diffusely into the adjacent parenchyma (especially frontal/temporal) and brainstem. Consistent with an inflammation spread "per continuitatem," the lateral cerebellar hemispheres and occipital poles, farthest away from the brain regions initially affected, remained largely unaffected until the final stages of the disease. Accompanying diffusion restriction of the T2-hyperintense lesions was common, as a possible surrogate for cytotoxic edema, whereas the blood–brain barrier was intact in most cases.

The dynamics of this pattern confirm previously published animal studies that showed a strong tropism of Bornaviridae for the cortical and subcortical gray matter, with only marginal white-matter involvement.[12] Although the clear path of infection and potential zoonotic spread still remain opaque, a theory of intranasal virus transmission with retrograde transaxonal migration to the brain has been proposed in horses and experimentally infected rats.[7,13] Speculative causes for this olfactory susceptibility include the direct contact of the olfactory nerves with the environment in addition to the lack of protective nerve sheathing, with a consequently delayed immune response.[14] Partly in line with these reports, and keeping in mind that the olfactory bulb per se is difficult to visualize on MRI, the gyrus rectus that runs along the olfactory bulb showed a common and early inflammatory involvement. Nonetheless, the alterations herein seem to have spread secondarily from the basal ganglia and not vice versa. Although highly speculative, the above-mentioned pattern of encephalitis on MRI could hence be explained more readily by an inflammation seeding through hematogenous rather than retrograde transaxonal spread.

Although the distribution pattern, with a predilection for the basal ganglia, can help in the differentiation from the more common herpes simplex virus type 1 (HSV-1) or autoimmune encephalitis, the lack of microhemorrhages differs from a typical late-stage finding in both HSV-1 and Japanese encephalitis.[15] The symmetric inflammation pattern in Borna encephalitis can also facilitate differentiation from HSV-1 encephalitis, in which mostly asymmetric involvement of the temporal lobes can be seen.[16]

In spite of the generally biphasic and benign course of tick-borne encephalitis, its overlapping endemic regions and comparable flu-like initial symptoms can mimic the characteristics of BoDV-1 encephalitis.[17] MRI abnormalities, which occur in only a minority of tick-borne encephalitis cases, can be seen in the thalamus and basal ganglia, but often also manifest themselves in the infratentorial region, with typical alterations of the cerebral crus and cerebellum.[18,19] The frequently associated leptomeningeal contrast enhancement and lack of parenchymal restriction of diffusion also facilitate differentiation from BoDV-1 encephalitis[19] (for comparison of BoDV-1 encephalitis with differential diagnoses, see Table 4).

Strikingly, the preference for the head of the caudate nucleus and striatum, with regularly associated restriction of diffusion along the cortical band (apparent in one-quarter of both early- and late-stage BoDV-1 encephalitis cases), resembles the typical MRI appearance of sporadic Creutzfeldt–Jakob disease (sCJD).[20,21] Further analogies with sCJD, such as the dramatically high lethality rates, are, however, counterbalanced by the faster disease course, with flu-like symptoms, in BoDV-1 encephalitis and the fact that imaging abnormalities tend to occur much earlier in the course of sCJD versus BoDV-1 encephalitis.[20] Furthermore, the occasional contrast enhancement of encephalitic lesions in BoDV-1 patients is an MRI phenomenon practically never encountered in sCJD.[22] Although 14-3-3 protein could be detected in 4 of the 16 patients in whom this test was performed, the sometimes-held conviction of its specificity for sCJD has long been rebutted, because this cerebrospinal fluid (CSF) marker is known to increase in various types of conditions with severe neurological damage, such as encephalitis.[23]

Rapidly occurring death in BoDV-1 encephalitis renders reliable comparison with the fulminant brain atrophy in sCJD impossible. Nonetheless, the T1-hyperintense transformation of the basal ganglia (an unexpected observation made in nearly half of our patients), which has also been reported in sCJD, deserves consideration. Explanations for this phenomenon in the basal ganglia are manifold and concurring, but the shortened longitudinal relaxation and subsequent increase in T1 signal can, in summary, be attributed to heightened tissue concentrations of either fat or paramagnetic ions, such as manganese or ferrous blood compounds. As shown by the dynamics on MRI, it seems

TABLE 4. Head-to-Head Comparison of BoDV-1 Encephalitis with Differential Diagnoses

Entity	Symptoms	1. Similar features to BoDV-1 encephalitis on MRI 2. Different features from BoDV-1 encephalitis on MRI	Natural course
BoDV-1 encephalitis	Flu-like symptoms, fever. Gait ataxia, dysphagia, blurred speech, hemiparesis, seizures	1. Latency of imaging abnormalities to clinical symptoms. Characteristic appearance, with initial predilection for the head of the caudate nucleus, insula, striatum and limbic regions. Subsequent spread, with typical sparing of the occipital region and cerebellar hemispheres. T1-hyperintense transformation of the basal ganglia in late-stage encephalitis 2. Not applicable	Rapidly progressing, with death occurring at a mean of 40 days
sCJD	Rapid cognitive decline, ataxia, akinetic muscular mute state[23]	1. T2w- and DWI abnormalities of the cerebral cortex, usually sparing the perirolandic area.[20] Involvement of the caudate nucleus and putamen, with anterior-to-posterior gradient.[21] T2w hyperintensities of the pulvinar (vCJD)[24] 2. Changes may precede clinical symptoms.[20] Rapidly progressing (cerebellar) atrophy.[21] Involvement of the occipital cortex and generally sparing the insula.[25,26]	Fatal condition, with death occuring at a mean of 6 mo
HSV-1	Prodromal state with fever, followed by seizures, abnormal behavior, disorientation[27]	1. T2w hyperintensity and diffusion restriction in the mesiotemporal and frontal lobes[15] 2. Basal ganglia tend to be spared. Mostly asymmetric. Changes usually visible 2–3 days after symptom onset.[28] T2* blooming as microhemorrhages occur	70% mortality if untreated, neuropsychiatric deficits common[27]
Japanese encephalitis	From nonspecific febrile illness to poliomyelitis-like paralysis[29]	1. Symmetric T2w hyperintensity, generally without restricted diffusion (in the acute stage) of the thalamus, basal ganglia and the brainstem. T1-hyperintense basal ganglia, attributable to hemorrhage. MRI can be negative ≤3 weeks after symptom onset 2. T2* blooming in the later stages.[30]	Neuropsychiatric sequalae in 50%, death in 25–30% of cases[29]
Dengue encephalitis	Fever, headache, retro-orbital pain. Myalgia and arthralgia	1. Involvement of the bilateral thalami, pallidum, temporal lobe, and hippocampus, with T2w hyperintensity, variable diffusion restriction, and variable contrast enhancement[31] 2. Lack of imaging abnormalities in ≤42% of cases[31]	Self-limiting, with good patient recovery in most cases
Tick-borne encephalitis	Biphasic clinical coursem with initial flu-like symptoms[17]	1. T2-hyperintense lesions in the thalamus (especially pulvinar), putamen, and crus cerebri.[18,19] 2. Imaging abnormalities in only a minority of cases. Affection of the cerebellum. Leptomeningeal enhancement. No parenchymal diffusion restriction[19]	Mostly favorable outcome
West Nile encephalitis	Fever/hypothermia, encephalopathy, acute onset of limb weakness[32]	1. Predilection for deep gray matter structures and basal ganglia. Diffusion restriction common. Normally, no contrast enhancement[33] 2. Involvement of the brainstem and cerebellum. No findings on neuroimaging in ~30% of cases[33,34]	High short-term mortality (18%), only 21% returning to previous levels of function[35,36]

The table shows the typical respective symptoms, commonalities, and differences on MRI, in addition to the natural disease course.
BoDV-1 = classical Borna disease virus, species *Mammalian 1 orthobornavirus*; HSV-1 = herpes simplex virus type 1; MRI = magnetic resonance imaging; sCJD = sporadic Creutzfeldt–Jakob disease; vCJD = variant Creutzfeldt–Jakob disease.

plausible that inflammation and thus tissue damage in BoDV-1 encephalitis is most prominent in the basal ganglia. Taken together with histological analyses that have confirmed a high concentration of macrophages in these regions, we hypothesize that late-stage necrosis leads to a transformation of microglia into lipid phagocytes and thus translates to this characteristic imaging appearance, a phenomenon previously known to occur in hypoxic–ischemic brain injury.[24]

In conclusion, this study provides the first comprehensive insight into the MRI morphology of BoDV-1 encephalitis. A characteristic pattern can be identified in both the early and late stages of the disease, with inflammation spreading from the head of the caudate nucleus, striatum, insula, and limbic system into the surrounding parenchyma. T1-hyperintense transformation of the basal ganglia is a common finding in the days preceding death, indicating macrophage infiltration into the most affected necrotic zones.

Although it is pathophysiologically different, the similar MRI features and equally devastating clinical course render differentiation from sCJD difficult and raise the question of whether BoDV-1 might be found retrospectively in prion-suspected brain samples that tested negative for sCJD.

Acknowledgments

No funding source was involved in the conception or carrying out of this study.

This study is dedicated to Georg Gosztonyi, a pioneer in Borna-related research.

We thank Thomas Ebersberger and Hans-Peter Dinkel for contributing MRI studies of 3 patients from community hospitals. We are also grateful for the support of Bernhard Neumann, who supplied clinical data of some patients. Open access funding enabled and organized by Projekt DEAL.

Author Contributions

Conception and design of study: C.Z., C.W., B.W., I.W., F.L.-S., T.F., F.D., J.S., and M.P. Data acquisition and analysis: F.L.-S., I.W., M.P., T.F., V.R., K.A., S.B., F.D., B.W., and C.Z. Drafting of the manuscript: T.F., F.L.-S., I.W., B.W., and C.Z. All authors have read and approved the final manuscript.

Bornavirus-Encephalitis Study Group: Drs A. Berlis, C. Maurer, M. Holtmannspötter, S. Wunderlich, M. Rosati, and D. Rubbenstroth.

Potential Conflicts of Interest

The authors have no conflicts of interest to report.

References

1. Liesche F, Ruf V, Zoubaa S, et al. The neuropathology of fatal encephalomyelitis in human Borna virus infection. Acta Neuropathol 2019;138:653–665.
2. Coras R, Korn K, Kuerten S, et al. Severe bornavirus-encephalitis presenting as Guillain-Barre-syndrome. Acta Neuropathol 2019;137:1017–1019.
3. Schlottau K, Forth L, Angstwurm K, et al. Fatal encephalitic Borna disease virus 1 in solid-organ transplant recipients. N Engl J Med 2018;379:1377–1379.
4. Korn K, Coras R, Bobinger T, et al. Fatal encephalitis associated with Borna disease virus 1. N Engl J Med 2018;379:1375–1377.
5. Niller HH, Angstwurm K, Rubbenstroth D, et al. Zoonotic spillover infections with Borna disease virus 1 leading to fatal human encephalitis, 1999-2019: an epidemiological investigation. Lancet Infect Dis. 2020;20:467–477.
6. Ludwig H. The biology of bornavirus. APMIS Suppl 2008;124:14–20.
7. Gosztonyi G. Natural and experimental Borna disease virus infections-neuropathology and pathogenetic considerations. APMIS Suppl 2008;124:53–57.
8. Boyko OB, Burger PC, Shelburne JD, Ingram P. Non-heme mechanisms for T1 shortening: pathologic, CT and MR elucidation. AJNR Am J Neuroradiol 1992;13:1439–1445.
9. Wang F, Flanagan J, Su N, et al. RNAscope: a novel in situ RNA analysis platform for formalin-fixed, paraffin-embedded tissues. J Mol Diagn 2012;14:22–29.
10. Bestetti G. Microscopic and ultrastructural studies on Joest-Degen inclusion bodies in spontaneous Borna disease of the horse. Schweiz Arch Tierheilkd 1976;118:493–498.
11. Rott R, Becht H. Natural and experimental Borna disease in animals. Curr Top Microbiol Immunol 1995;190:17–30.
12. Maclachlan NJ, Dubovi EJ, Barthold SW, et al. *Fenner's veterinary virology*. 5th ed. Amsterdam: Elsevier/AP, Academic Press is an imprint of Elsevier, 2017 xix, 581.
13. Kupke A, Becker S, Wewetzer K, et al. Intranasal Borna disease virus (BoDV-1) infection: insights into initial steps and potential Contagiosity. Int J Mol Sci 2019;20:1318.
14. Detje CN, Lienenklaus S, Chhatbar C, et al. Upon intranasal vesicular stomatitis virus infection, astrocytes in the olfactory bulb are important interferon Beta producers that protect from lethal encephalitis. J Virol 2015;89:2731–2738.
15. Sawlani V. Diffusion-weighted imaging and apparent diffusion coefficient evaluation of herpes simplex encephalitis and Japanese encephalitis. J Neurol Sci 2009;287:221–226.
16. Kim YS, Jung KH, Lee ST, et al. Prognostic value of initial standard EEG and MRI in patients with herpes simplex encephalitis. J Clin Neurol 2016;12:224–229.
17. Kaiser R. The clinical and epidemiological profile of tick-borne encephalitis in southern Germany 1994-98: a prospective study of 656 patients. Brain 1999;122:2067–2078.
18. Pichler A, Sellner J, Harutyunyan G, et al. Magnetic resonance imaging and clinical findings in adults with tick-borne encephalitis. J Neurol Sci 2017;375:266–269.
19. Horger M, Beck R, Fenchel M, et al. Imaging findings in tick-borne encephalitis with differential diagnostic considerations. AJR Am J Roentgenol 2012;199:420–427.

20. Ukisu R, Kushihashi T, Kitanosono T, et al. Serial diffusion-weighted MRI of Creutzfeldt-Jakob disease. AJR Am J Roentgenol 2005;184: 560–566.

21. Meissner B, Westner IM, Kallenberg K, et al. Sporadic Creutzfeldt-Jakob disease: clinical and diagnostic characteristics of the rare VV1 type. Neurology 2005;65:1544–1550.

22. Rudge P, Hyare H, Green A, et al. Imaging and CSF analyses effectively distinguish CJD from its mimics. J Neurol Neurosurg Psychiatry 2018;89:461–466.

23. Hsich G, Kenney K, Gibbs CJ, et al. The 14-3-3 brain protein in cerebrospinal fluid as a marker for transmissible spongiform encephalopathies. N Engl J Med 1996;335:924–930.

24. Brierley JB, Brown AW. The origin of lipid phagocytes in the central nervous system: I. the intrinsic microglia. J Comp Neurol 1982;211: 397–406.

25. Otto A, Zerr I, Lantsch M, et al. Akinetic mutism as a classification criterion for the diagnosis of Creutzfeldt-Jakob disease. J Neurol Neurosurg Psychiatry 1998;64:524–528.

26. Collie DA, Summers DM, Sellar RJ, et al. Diagnosing variant Creutzfeldt-Jakob disease with the pulvinar sign: MR imaging findings in 86 neuropathologically confirmed cases. AJNR Am J Neuroradiol 2003;24:1560–1569.

27. Tsuji Y, Kanamori H, Murakami G, et al. Heidenhain variant of Creutzfeldt-Jakob disease: diffusion-weighted MRI and PET characteristics. J Neuroimaging 2004;14:63–66.

28. Sili U, Kaya A, Mert A, Group HSVES. Herpes simplex virus encephalitis: clinical manifestations, diagnosis and outcome in 106 adult patients. J Clin Virol 2014;60:112–118.

29. Bulakbasi N, Kocaoglu M. Central nervous system infections of herpesvirus family. Neuroimaging Clin N Am 2008;18:53–84. viii.

30. Solomon T, Dung NM, Kneen R, et al. Japanese encephalitis. J Neurol Neurosurg Psychiatry 2000;68:405–415.

31. Shoji H, Kida H, Hino H, et al. Magnetic resonance imaging findings in Japanese encephalitis. White matter lesions. J Neuroimaging 1994;4:206–211.

32. Vanjare HA, Mannam P, Mishra AK, et al. Brain imaging in cases with positive serology for dengue with neurologic symptoms: a Clinicoradiologic correlation. AJNR Am J Neuroradiol 2018;39: 699–703.

33. Sejvar JJ, Haddad MB, Tierney BC, et al. Neurologic manifestations and outcome of West Nile virus infection. JAMA 2003;290:511–515.

34. Petropoulou KA, Gordon SM, Prayson RA, Ruggierri PM. West Nile virus meningoencephalitis: MR imaging findings. AJNR Am J Neuroradiol 2005;26:1986–1995.

35. Ali M, Safriel Y, Sohi J, et al. West Nile virus infection: MR imaging findings in the nervous system. AJNR Am J Neuroradiol 2005;26: 289–297.

36. Bode AV, Sejvar JJ, Pape WJ, et al. West Nile virus disease: a descriptive study of 228 patients hospitalized in a 4-county region of Colorado in 2003. Clin Infect Dis 2006;42:1234–1240.